Chemical Science

ROYAL SOCIETY OF CHEMISTRY

EDGE ARTICLE

View Article Online
View Journal | View Issue

Cite this: *Chem. Sci.*, 2025, **16**, 3329

All publication charges for this article have been paid for by the Royal Society of Chemistry

Different p-block elements induce C_3[111] octahedral distortion in titanium to generate an intense nonlinear effect†

Zhenhua Li,‡[a] Zhengli Liang,‡[b] Jiahao Wan,[a] Lehui Liu,[c] Chunxiang Wu,[a] Ping Wang,[a] Xingxing Jiang,*[b] Zheshuai Lin[b] and Hongming Liu*[a]

Received 30th September 2024
Accepted 14th January 2025

DOI: 10.1039/d4sc06620k

rsc.li/chemical-science

Acentric crystalline materials are the cornerstone of numerous cutting-edge technologies and have been highly sought-after, but they are difficult to construct controllably. Herein, by introducing a new p-block element to break the symmetrical environment of the d^0 transition metal in the centric matrix $TiTe_3O_8$, a novel acentric tellurite sulfate, namely $Ti(TeO_3)(SO_4)$, was successfully constructed. In its structure, two types of p-block element-centered oxo-anionic groups, *i.e.* $[TeO_3]$ and $[SO_4]$, endow $[TiO_6]$ with an out-of-center distortion along the local C_3[111] direction, which is rare in titanium oxides containing a lone-pair cation. The synergy of the distorted $[TiO_6]$ octahedron, lone-pair $[TeO_3]$ pyramid and rigid $[SO_4]$ tetrahedron within its structure induces a strong second harmonic generation (SHG) response of 11.6 × KDP (KH_2PO_4), the largest value among mercury-free sulfates. Additionally, $Ti(TeO_3)(SO_4)$ also shows the largest birefringence (0.145) among sulfates possessing an SHG response that is more than ten times that of KDP, showing huge potential as a nonlinear optical material. The successful implementation of the strategy of inducing intra-octahedral distortion in a d^0 transition metal by different p-block elements provides new opportunities for constructing acentric structures and exploiting outstanding nonlinear optically active sulfates.

Introduction

Crystalline materials featuring a non-centrosymmetric (NCS) structure are the cornerstone of some crucial properties such as piezoelectricity, ferroelectricity, second-order nonlinear optical (NLO) phenomena, and dielectric behavior.[1–3] Among these properties, the second-order NLO effect is the key to the frequency conversion of solid-state laser devices.[4–11] Though acentric crystals are highly sought after for their fascinating versatility, the vast majority of inorganic compounds have a tendency to crystallize in the centric space groups. Over the past few decades, numerous strategies have been proposed to facilitate the construction of NCS structures, *e.g.*, the combination of multiple anionic groups,[12–14] cation compensation,[15,16] multi-component modification,[17] heterovalent substitution,[18–21] the condensation of anionic units,[22–24] *etc.*[25–31] Their implementation gave rise to the discovery of plentiful NLO crystals that demonstrate outstanding performance. However, the application of these strategies does not always ensure the formation of an NCS structure. Generally, the symmetric arrangement of anionic groups within the structure still leads to a centric space group. The crucial step in constructing NCS structures lies in designing more practical and feasible strategies to directly disrupt the spatially symmetric alignment.

According to the anionic group theory,[32,33] the macroscopic second harmonic generation (SHG) effect of NLO crystals stems from the geometric addition of the microscopic second-order susceptibility tensor of the NLO-active basic building units (BBUs) within the structure. Distorted octahedra consisting of a d^0 transition metal (M^{d0}) bonded to six O atoms ($M^{d0}O_6$) represent a category of NLO-active BBUs with spontaneous polarization; the introduction of these units facilitates the formation of NCS structures and may potentially lead to a strong SHG response.[34–37] Therefore, the combination of distorted $[M^{d0}O_6]$ with other NLO-active BBUs has been widely applied to construct NLO crystals, including iodate, selenite, tellurite, and germanate.[38–44] For $[M^{d0}O_6]$ octahedra, most of

[a]*Guangxi Key Laboratory of Electrochemical Energy Materials, School of Chemistry and Chemical Engineering, Guangxi University, Nanning, Guangxi 530004, China. E-mail: hongming9224@126.com*

[b]*Technical Institute of Physics and Chemistry, Chinese Academy of Science, Beijing 100190, China. E-mail: xxjiang@mail.ipc.ac.cn*

[c]*Key Laboratory of Optoelectronic Materials Chemistry, Physics Fujian Institute of Research on the Fujian, Fuzhou, 350002, China*

† Electronic supplementary information (ESI) available: Experimental, crystallographic data, information on some sulfates, XRD patterns, EDS data, IR spectrum, additional crystal structure, TG-DSC curves, crystal photos, UV-vis-NIR spectra, dipole moment calculation, and computational results. CCDC 2364994 contains the supplementary crystallographic data for $Ti(TeO_3)(SO_4)$. For ESI and crystallographic data in CIF or other electronic format see DOI: https://doi.org/10.1039/d4sc06620k

‡ These authors contributed equally.

their out-of-center distortion can be ascribed to the second-order Jahn–Teller (SOJT) electronic effect,[45,46] which is categorized as a primary distortive effect and occurs when the empty d-orbitals of the metal mix with the filled p-orbitals of the ligands.[35] Further, the intra-octahedral distortion of $[M^{d0}O_6]$ can also be influenced by the bond networks and lattice stresses from other directly connected oxo-anionic groups, which is called secondary distortion.[35] Normally, the secondary distortion is weaker and serves to enhance the primary distortion, as reflected by the M^{d0}-oxides containing a lone-pair cation. When an $[M^{d0}O_6]$ octahedron bridges both the lone-pair cation and other $[M^{d0}O_6]$ octahedra simultaneously, an intra-distortion is highly likely to occur (Fig. 1a). Nevertheless, the secondary distortion can sometimes override the primary distortion, as exemplified by the $[TiO_6]$ octahedron in the winstanleyite $TiTe_3O_8$,[47] and its out-of-center distortion is inhibited due to the coordination with six identical $[TeO_4]$ polyhedra. This symmetric configuration is unfavorable to the formation of acentric structures.

For those $[M^{d0}O_6]$ octahedra with repressed distortion, introducing an additional BBU to break their symmetric coordination may be a viable route to activate their secondary distortion. In order to explore the feasibility of this assumption, the aforementioned centric $TiTe_3O_8$ was selected as the matrix. In terms of the selection of appropriate BBUs, the tetrahedral $[PO_4]$, $[SO_4]$, and $[SiO_4]$ came into our sight for the following reasons: (1) tetrahedral BBUs can also exert a profound influence on the intra-octahedral distortion of $[M^{d0}O_6]$, as exemplified by $KTiOPO_4$.[48] Additionally, we systematically examined the distortion characteristics of the $[M^{d0}O_6]$ octahedra in phosphates, sulfates, and silicates containing M^{d0}, and the result showed that inside the $[M^{d0}O_6]$ octahedra, the length of the M^{d0}–O bonds connecting to the tetrahedral groups differed greatly from that connecting to other $[M^{d0}O_6]$ octahedra, which induced universal distortion inside the $[M^{d0}O_6]$ octahedra (Fig. 1b and S1†), just as the situation of the intra-octahedral $[M^{d0}O_6]$ distortion in M^{d0}-oxides containing a lone-pair cation.[35] (2) The introduced tetrahedral groups are expected to induce a symmetry-breaking of the $[TiO_6]$ coordination (Fig. 1a), and the subsequently distorted $[TiO_6]$ unit can act as an NLO-active BBU to participate in the SHG response contribution of the target crystals. (3) The introduction of tetrahedral groups may also break the symmetric arrangement of the $[TeO_4]$ polyhedra in the $TiTe_3O_8$ structure and give rise to a surprisingly strong SHG in the resulting phosphates, sulfates, or silicates, as most of them are beset with low SHG intensities owing to the small polarizability of $[PO_4]$, $[SO_4]$, and $[SiO_4]$ tetrahedra.

Following the strategy of introducing a tetrahedral unit into the structure of $TiTe_3O_8$, a novel tellurite–sulfate, namely $Ti(TeO_3)(SO_4)$, was synthesized. It represents a rare M^{d0}-containing acentric crystal where the $[M^{d0}O_6]$ octahedron directly connects to both the tetrahedral anionic group and lone-pair cation, and it is also a rare titanium oxide in which the $[TiO_6]$ octahedron is linked to lone-pair cations but features C_3[111] (face) distortion, which results from its simultaneous connection with two types of p-block elements, Te and S. Furthermore, experimental and calculational investigations suggest that the unique distorted $[TiO_6]$ octahedron collaborates with the $[TeO_3]$ and $[SO_4]$ groups, giving rise to an intense SHG response of 11.6 × KDP for $Ti(TeO_3)(SO_4)$, which is the maximum among mercury-free sulfates.

Results and discussion

Pure $Ti(TeO_3)(SO_4)$ crystals were prepared *via* a hydrothermal process at 230 °C with raw materials of TiO_2, TeO_2, and sulfuric acid solution. The purity of the synthetic samples was confirmed by powder X-ray diffraction (XRD) analysis (Fig. S2†). Energy-dispersive X-ray spectroscopy (EDS) performed on $Ti(TeO_3)(SO_4)$ crystals suggests an average molar ratio of 1.08 : 1.16 : 1 : 7.15 for Ti, Te, S, and O elements (Fig. S3†), matching well with the chemical formula determined by single-crystal XRD. The IR spectrum of $Ti(TeO_3)(SO_4)$ powder shows no

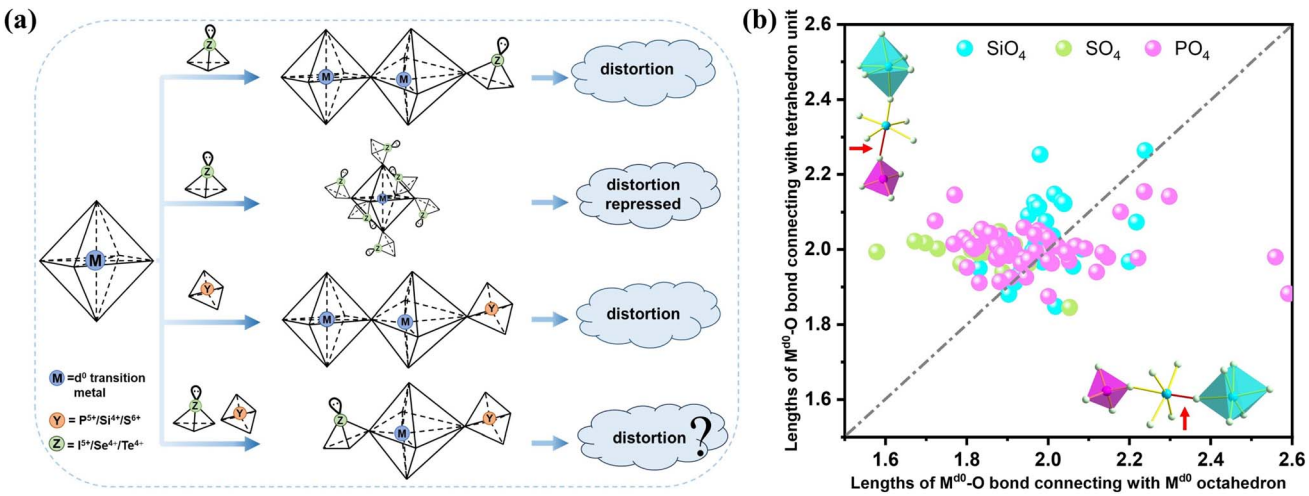

Fig. 1 (a) Schematic diagram of $[M^{d0}O_6]$ octahedral distortion induced by different connections. (b) Length distribution of M^{d0}–O bonds in the $[M^{d0}O_6]$ octahedron connected to other $[M^{d0}O_6]$ octahedra and tetrahedral units simultaneously in phosphates, sulfates, and silicates containing M^{d0}.

obvious absorption in the range of 4000–1370 cm^{-1} (Fig. S4†), and the absorption peaks between 1200 and 950 cm^{-1} can be attributed to the stretching vibrations of S–O bonds, accurately proving the existence of the [SO_4] tetrahedron, while these peaks between 900 and 620 cm^{-1} are assigned to the stretching vibration of Te–O and Ti–O bonds. These assignments are consistent with the reported articles.

Single-crystal XRD determination shows that $Ti(TeO_3)(SO_4)$ crystallizes into the NCS space group $P2_1$ (Table S1†). There are crystallographically independent one Te atom, one S atom, one Ti atom, and seven O atoms in its asymmetric unit (Table S2†). Bond valence sum (BVS) calculation[49] yields values of 4.34, 6.07 and 3.96 for Ti, S and Te atoms, respectively (Table S2†), matching well with their oxidation states. All these atoms are located in ordinary positions (Fig. S5†). As shown in Fig. 2a, the Te atom is bonded with three O atoms to form a [TeO_3] pyramid containing lone-pair electrons, with the Te–O bond lengths ranging from 1.858 Å to 1.897 Å (Table S3†). The S atom coordinates with four O atoms to form a typical [SO_4] tetrahedron with the S–O bond lengths in the range of 1.459–1.476 Å. The Ti atom is coordinated by six O atoms to compose a typical [TiO_6] octahedron with three long (2.018–2.072 Å) and three short (1.813–1.876 Å) Ti–O bonds. According to the classification proposed by Halasyamani,[35] the out-of-center distortion of the [TiO_6] octahedron in this structure belongs to the C_3[111] direction. To our knowledge, this C_3[111] distortion is rare in Ti^{4+} oxides containing a lone-pair cation. Further structural analysis indicates that the three long Ti–O bonds are linked by [SO_4] groups, while the three short ones are connected by [TeO_3] groups (Fig. S6†). This implies that the C_3[111] distortion in the [TiO_6] octahedron in this structure results from the connection of Ti–O bonds to different types of p-block element-centered oxo-anionic groups. It breaks the existing view that, for the M^{d0} oxides containing a lone-pair cation, the intra-octahedral distortion of [$M^{d0}O_6$] only occurs when it directly connects with at least one other M^{d0} cation or contains at least one terminal O atom.[35] The [TiO_6] octahedron links with three [SO_4] groups and three [TeO_3] groups (Fig. 2b), and both the [TeO_3] pyramid and [SO_4] tetrahedron are three-connected by [TiO_6] octahedra, with the remaining O atom in the [SO_4] group being pensile alone (Fig. S6†). The [TiO_6] octahedra and [TeO_3] pyramids are interlaced to form a [$(TiO_3O_{3/2})(TeO_{3/2})$] layer parallel to the *ab*-plane (Fig. 2d). The [$(TiO_3O_{3/2})(TeO_{3/2})$] layers are stacked along the *c*-axis through the connection of [SO_4] tetrahedra to build the final three-dimensional structure of $Ti(TeO_3)(SO_4)$ (Fig. 2c). In the connection mode, it can be characterized to [$(TiO_{6/2})(TeO_{3/2})(SO_{3/2}O)$].

A detailed structural comparison suggests that the introduction of the [SO_4] group leads to obvious structural changes in contrast to the matrix $TiTe_3O_8$. Firstly, the introduced [SO_4] groups substitute three of the six [TeO_4] groups surrounding the [TiO_6] octahedron (Fig. 2e, b), and the remaining three [TeO_4] groups with relatively small local dipole moment (LDM, μ_c = 11.5 *D*) are also converted to [TeO_3] groups with larger LDM (μ_c = 12.2 *D*) (Fig. 2a). Secondly, the [SO_4] groups combined with the [TeO_3] groups induce the C_3[111] distortion of the [TiO_6] octahedron in $Ti(TeO_3)(SO_4)$ (Fig. 2b), which is different from the undistorted [TiO_6] octahedron in $TiTe_3O_8$ (Fig. 2e). The magnitude of out-of-center distortion (Δd) calculated by the method proposed by Halasyamani[35] gives a value of $\Delta d = 0.62$ for the [TiO_6] octahedron in $Ti(TeO_3)(SO_4)$, which can be quantified as moderate distortion. This value is much larger than the average magnitude of Ti^{4+} ($\Delta d = 0.34$), which is often considered to be a weak distorter and is the weakest distorted M^{d0} cation among Mo^{6+}, V^{5+}, W^{6+}, Nb^{5+}, Ta^{5+} and Ti^{4+}.[35] A reasonable spatial arrangement of such distorted [TiO_6] octahedra within the structure is expected to enhance the NLO effect of the resultant $Ti(TeO_3)(SO_4)$. Thirdly, the introduction of [SO_4]

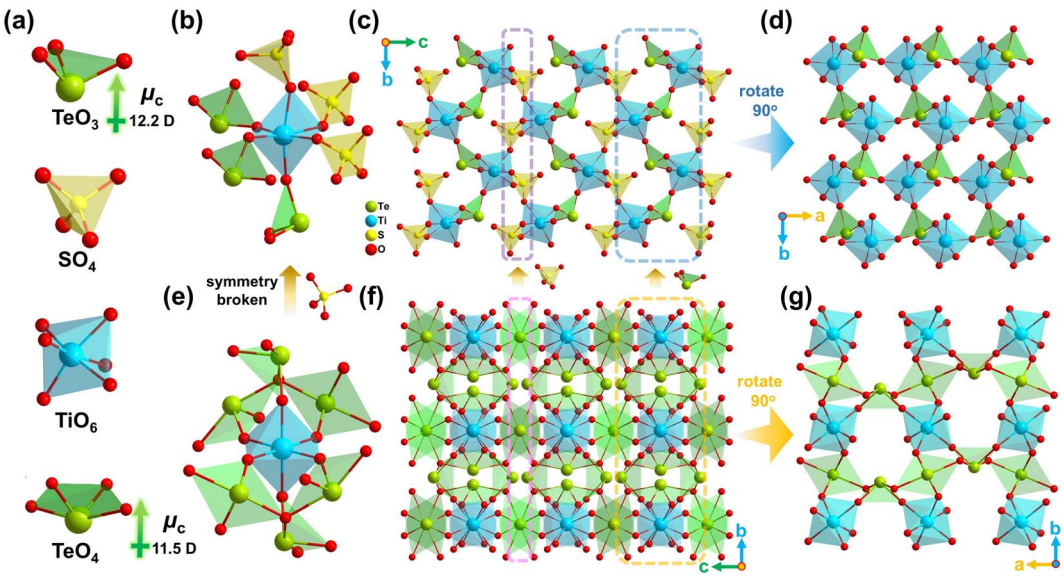

Fig. 2 Structural diagram of $Ti(TeO_3)(SO_4)$ and $TiTe_3O_8$. (a) The anionic groups; $Ti(TeO_3)(SO_4)$ structure: (b) the $Ti(TeO_3)_3(SO_4)_3$ unit, (c) the structure viewed along the [100] direction, (d) the [$(TiO_3O_{3/2})(TeO_{3/2})$] layer viewed along the [001] direction; $TiTe_3O_8$ structure: (e) the coordination environment of [TiO_6], (f) the structure viewed along the [100] direction, (g) the [$(TiO_2O_{4/2})(TeO_{4/2})_2$] layer viewed along the [001] direction.

groups also changes the arrangement of the lone-pair anionic groups. As shown in Fig. 2f and g, the structure of $TiTe_3O_8$ can be seen as the stacking of $[(TiO_2O_{4/2})(TeO_{4/2})_2]$ layers along the *c*-axis through the interlayer connection of $[TeO_4]$ groups, while the structure of $Ti(TeO_3)(SO_4)$ can be approximately regarded as a derivation of the $TiTe_3O_8$ structure, obtained by replacing the interlayer $[TeO_4]$ groups with the $[SO_4]$ groups, and the $[TeO_4]$ groups within the layer are replaced by the $[TeO_3]$ groups (Fig. 2c). All the $[TeO_4]$ groups are anti-parallelly oriented in the $TiTe_3O_8$ structure (Fig. 2f and g). Combined with the symmetric $[TiO_6]$ octahedron, it crystallizes in the cubic $Ia\bar{3}$ space group.[47] However, the introduced $[SO_4]$ groups break the highly symmetric arrangement of the $[TeO_4]$ groups, leading to a non-antiparallel orientation of the $[TeO_3]$ groups (Fig. 2c and d), and ultimately result in symmetry-breaking in the structure of $Ti(TeO_3)(SO_4)$. The $[TeO_3]$ groups in its structure have a distinct net polarization vector on the *b*-axis. This will undoubtedly lead to a drastic change in the optical properties of $Ti(TeO_3)(SO_4)$ compared to $TiTe_3O_8$. In addition, the composition of $Ti(TeO_3)(SO_4)$ implies its possible similarities to TiO_2 polymorphs. Comparative analysis of structures suggests that $Ti(TeO_3)(SO_4)$ can be regarded as a derived product of rutile TiO_2, which is obtained by replacing half of the O atoms of the $[TiO_6]$ octahedron with $[TeO_3]$ units and the other half of the O atoms with $[SO_4]$ units in its structure (Fig. S7†).

Powder SHG measurement shows that the SHG intensity of $Ti(TeO_3)(SO_4)$ enhances gradually as the particle size increases under 1064 nm laser irradiation, implying that it is type-I phase-matching at 1064 nm (Fig. 3a).[50] Furthermore, it exhibits a strong SHG intensity that is about 11.6 times that of the reference KDP (Fig. 3b). The calculated SHG tensors (Table S4†) taking into account the constraints of Kleinman's symmetry and the space group ($P2_1$) also afford a large value ($d_{222} = 3.16$ pm V^{-1}), in rough agreement with the measured value. As is known, due to the small microscopic second-order susceptibility tensor of the tetrahedral $[SO_4]$ unit, the majority of sulfates suffer from the issue of weak SHG intensity, despite several tactics having been implemented recently to enhance the SHG response of sulfate, such as introducing lone-pair and lanthanide-polyhedron anionic groups, which leads to the finding of improved SHG response of $CeF_2(SO_4)$ (8 × KDP),[51] $Te_2O_3(SO_4)$ (6 × KDP),[52] $K_2Bi_2(SO_4)_2Cl_4$ (5.5 × KDP),[53] $Rb_2Bi_2(SO_4)_2Cl_4$ (5.3 × KDP),[53] and $Nb_2O_3(IO_3)_2(SO_4)$ (6 × KDP).[42] Only two age-old mercury-based acentric crystals were lately found to possess SHG responses stronger than 10 × KDP, including $HgSO_4$ (11 × KDP)[54] and $Hg_3O_2SO_4$ (14 × KDP).[55] However, the presence of recognized highly toxic mercury will greatly limit their application expansion as NLO materials. By contrast, the application expansion of $Ti(TeO_3)(SO_4)$ only suffers from the concern about the suspected hazards of tellurium compounds such as teratogenicity.[56,57] Partial density of states (DOS) calculation reveals that the top of the valence band is dominated by the non-bonding O-2p and Te-5p orbitals from −7 eV to 0 eV, and the bottom of the conduction band is composed of the unoccupied Ti-3d and Te-5p orbitals located from +2 eV to +8 eV (Fig. S8†), suggesting that the Ti–O and Te–O interactions determine the strong SHG response of $Ti(TeO_3)(SO_4)$. The SHG-weighted electron density maps also show that the occupied and unoccupied states are mostly concentrated on the $[TiO_6]$ and $[TeO_3]$ units in the virtual electron process, but are nearly absent in the $[SO_4]$ groups (Fig. 3c and d), implying the predominant contribution of $[TiO_6]$ and $[TeO_3]$ groups to the strong SHG response of $Ti(TeO_3)(SO_4)$. This result is also supported by the local dipole moment (LDM) calculation.

As listed in Table S5,† the polarizations of the $[TiO_6]$, $[TeO_3]$, and $[SO_4]$ units entirely neutralize each other on the *x*- and *z*-components, while they are superimposed on the *y*-component,

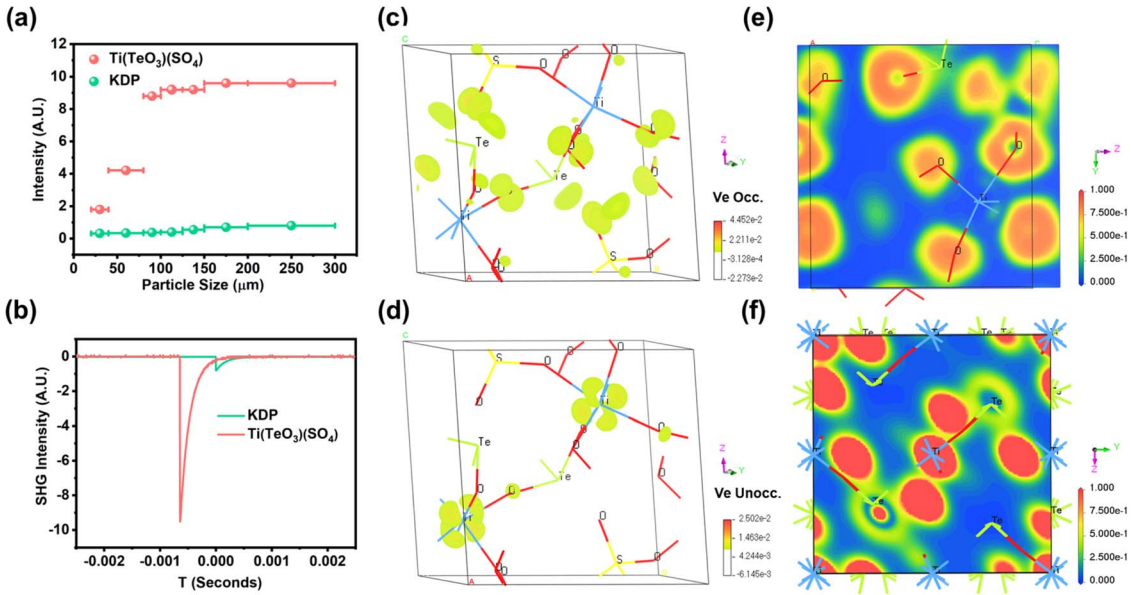

Fig. 3 (a) SHG intensity *versus* particle size under laser irradiation at 1064 nm with KDP as the reference; (b) oscilloscope traces of the SHG signals (at the sample size range of 200–300 μm); SHG-weighted density map of (c) occupied and (d) unoccupied states in the virtual electron process; calculated electron-density difference of (e) $Ti(TeO_3)(SO_4)$ (100) and (f) $TiTe_3O_8$ (100).

giving a total dipole moment of 16.864 *D* within the unit cell (Fig. S9†). This indicates that the strong SHG response of $Ti(TeO_3)(SO_4)$ can be ascribed to the synergy of the $[TiO_6]$ octahedron, $[TeO_3]$ pyramid, and $[SO_4]$ tetrahedron. It is a compound with an excellent SHG response obtained by the combination of three types of NLO-active BBUs. Taking into account the unit cell volume, the calculated density of dipole moment is 64.5×10^{-21} esu cm $Å^{-3}$ for $Ti(TeO_3)(SO_4)$. Contrastively, the same calculation approach gives the renowned NLO crystal $KTiOPO_4$ a dipole moment density of 32.9×10^{-21} esu cm $Å^{-3}$ (Table S6†). Additionally, the net dipole moments of the isolated $[TiO_6]$ and $[TeO_3]$ units were calculated to be 2.224 *D* and 15.842 *D*, respectively, contributing predominantly to the total dipole moment of $Ti(TeO_3)(SO_4)$. Besides, the electron density calculation results also reveal that the electron densities around Ti and O in $TiTe_3O_8$ are close (Fig. 3f). In stark contrast, an apparent difference in electron density is found around Ti and O in $Ti(TeO_3)(SO_4)$ (Fig. 3e). This implies that the introduction of an $[SO_4]$ tetrahedron enhances the polarization of the Ti–O covalent bonds, consistent with the high distortion and enhanced dipole moment of the $[TiO_6]$ octahedron in $Ti(TeO_3)(SO_4)$ compared to that in $TiTe_3O_8$. All the above analyses imply that $[TiO_6]$ and $[TeO_3]$ units could be enormously conducive to sulfates to generate a strong SHG response. This provides a novel avenue to achieve large NLO coefficients in sulfates.

For a potential NLO crystal, a large-enough birefringence (usually >0.02) is a requisite to guarantee its phase-matching character. Under a polarizing microscope, the observed interference color for a crystal plate with a thickness of 7.6 μm is II-order blue, corresponding to an optical path difference of about 1.1 μm (Fig. 4a),[58] so the measured birefringence is 0.145@visible light for $Ti(TeO_3)(SO_4)$. This value is competitive to those of most reported asymmetric sulfates (Table S7†). Among acentric sulfates possessing an SHG response stronger than 10 × KDP, $Ti(TeO_3)(SO_4)$ exhibits the largest birefringence (Fig. 4b), ensuring phase matchability of its crystal over a wide wavelength range. The DFT calculation gave a refractive index relationship of $n_{X1} > n_{X2} > n_{X3}$ between the three optical main axes, a birefringence of 0.137@1064 nm and the shortest phase-matchable wavelength of 413 nm (Fig. 4c), well consistent with the experimental results. As is known, most sulfates suffer from small birefringences owing to the weak optical anisotropy resulting from the nearly isotropic configuration of the tetrahedral $[SO_4]$ group, hence hindering their phase-matchability in the short wavelength region.[59,60] Compared with the non-birefringence characteristics of the matrix $TiTe_3O_8$ (isotropic cubic space group), the birefringence of $Ti(TeO_3)(SO_4)$ has gained a great enhancement. This confirms the superiority of the strategy of introducing the $[SO_4]$ unit to induce symmetry-breaking in developing large birefringent sulfates. In the structure of $Ti(TeO_3)(SO_4)$, the $[TiO_6]$ features an obvious out-of-center distortion ($\Delta d = 0.62$), while the $[TeO_3]$ possesses lone-pair and a large local dipole moment ($\mu_c = 12.2$ *D*), both of which exhibit larger optical anisotropy than the $[SO_4]$ group, hence the $[TiO_6]$ and $[TeO_3]$ groups contribute predominantly to its large birefringence, consistent with the results of some other sulfates.[42,51,61] The large birefrigence of some tellurites and TiO_2 crystal can support this speculation as well.[62,63]

Thermogravimetric analysis reveals that $Ti(TeO_3)(SO_4)$ can be stable up to 560 °C (Fig. S10†). The differential scanning calorimetry curve also illustrates that there is no phase transition prior to its decomposition, as verified by the powder XRD pattern of the samples after thermal annealing at 500 °C (Fig. S11†). Its stability is superior to that of most tellurite sulfates, as exemplified by $Te_2O_3SO_4$ (540 °C),[52] $Te(OH)_3(SO_4)\cdot H_3O$ (110 °C),[52] and $Y_3(TeO_3)_2(SO_4)_2(OH)(H_2O)$ (434 °C).[64] The powder XRD pattern of the calcined product at 700 °C shows that it decomposes into

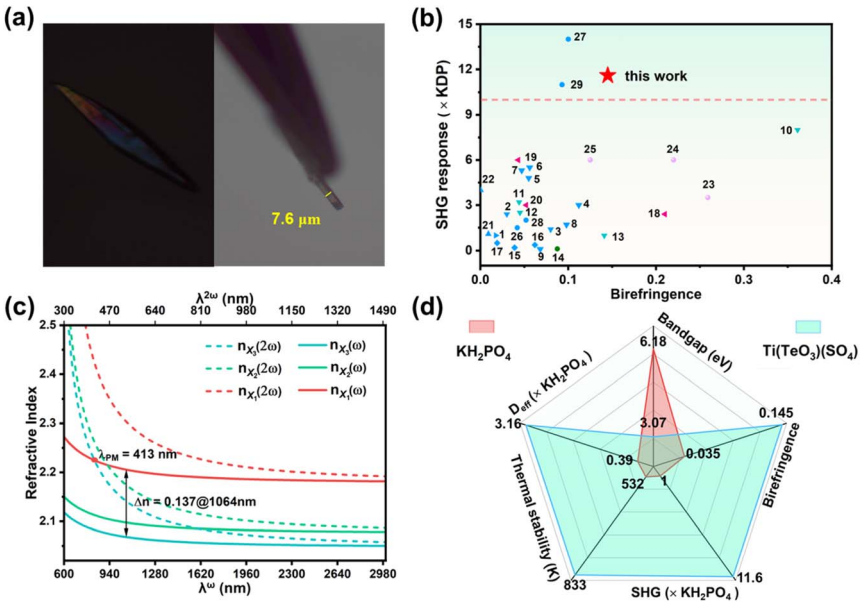

Fig. 4 (a) The original interference color under orthogonal polarized light and thickness of the selected crystal plate of $Ti(TeO_3)(SO_4)$; (b) SHG responses and birefringence of some reported sulfates (the numbers insides correspond to the serial numbers of the sulfates listed in Table S7†); (c) the calculated refractive index dispersion curves; (d) properties comparison of $Ti(TeO_3)(SO_4)$ with the commercial KH_2PO_4.

$TiTe_3O_8$ and TiO_2 (Fig. S12†). To find out the water, acid, and alkali resistance of $Ti(TeO_3)(SO_4)$, the morphological evolution of its crystals in pure water, 0.1 M nitric acid and 0.1 M sodium hydroxide solutions was recorded, respectively. The crystals preserve their full morphology and high transparency after being immersed either in water for 15 days or in an acid/alkali solution for 24 h (Fig. S13–S15†), and the PXRD patterns also remain unchanged (Fig. S16–S18†). This preliminarily result indicates that it has outstanding resistance to water-solubility as well as stability in acidic and alkaline environments. In addition, the SHG intensity of the powder samples also confirms that the water/acid/alkali environment will not weaken its NLO intensity (Fig. S19 and S20†), ensuring optical stability in multiple usage scenarios. The UV-vis-NIR spectrum indicates a UV cut-off edge of 312 nm for $Ti(TeO_3)(SO_4)$ (Fig. S21†), and the fitted Tauc plot gives a direct band gap of 3.61 eV and an indirect band gap of 3.07 eV (Fig. S22†). The calculated band structure diagram (Fig. S23†) shows that it is an indirect band gap ($D \rightarrow Y$) crystal, and the calculated value is 2.75 eV, a little lower than the experimental indirect band gap value (3.07 eV) due to the limitation of the DFT method. This band gap is clearly wider than that of the commercial NLO crystals $AgGaSe_2$ (1.83 eV) and $AgGaS_2$ (2.6 eV), and is comparable to some remarkable sulfates, such as $CeF_2(SO_4)$ (2.71 eV)[51] and $Nb_2O_3(IO_3)_2(SO_4)$ (3.25 eV).[42] A test on powder samples gives a laser damage threshold of up to 50 MW cm^{-2} for $Ti(TeO_3)(SO_4)$, which is 12.5 times higher than that of $AgGaS_2$ (4 MW cm^{-2}), in line with its wide band gap.[65]

Since $Ti(TeO_3)(SO_4)$ represents one of the NLO crystals with potential application value, its NLO-related properties were systematically compared with those of KH_2PO_4, one of the broadly applied SHG materials. The comparison focused on several key aspects: SHG intensity, birefringence, band gap, thermal stability, and NLO coefficient (d_{eff}). The results show that $Ti(TeO_3)(SO_4)$ presents an outstanding comprehensive performance as a potential NLO crystal (Fig. 4d).

Conclusions

By introducing an $[SO_4]$ group into a centric titanium tellurate, an acentric titanium-containing tellurate–sulfate, $Ti(TeO_3)(SO_4)$, was gained through a hydrothermal process. Within its three-dimensional structure, the $[TiO_6]$ octahedron is connected to three lone-pair $[TeO_3]$ pyramids and three $[SO_4]$ tetrahedra. The two types of p-block element-centered oxoanionic groups induce an out-of-center distortion in the $[TiO_6]$ along the local C_3[111] direction, which is rare in titanium oxides containing lone-pair cation. This also proves that the octahedral distortion of $[TiO_6]$ in titanium oxides containing a lone-pair cation can also be induced by the direct attachment of two types of p-block elements, rather than by the requisite involvement of a $[TiO_6]$ octahedron or terminal O atom as previously thought. $Ti(TeO_3)(SO_4)$ exhibits the strongest second harmonic generation response (11.6 × KDP) among mercury-free sulfates and a large birefringence (0.145) owing to the favorable arrangement of the $[TiO_6]$ octahedron, $[TeO_3]$ pyramid, and $[SO_4]$ tetrahedron within the structure, suggesting its high application potential as an NLO material. This work also paves the way for the design of novel NLO materials by introducing various p-block elements to induce distortion in $[M^{d0}O_6]$ units, thereby potentially achieving a strong SHG response.

Data availability

The data supporting this article have been included as part of the ESI.† Crystallographic data for 2364994 have been deposited at the CCDC.

Author contributions

Zhenhua Li: conceptualization, investigation, data curation, and writing – original draft; Zhengli Liang: data curation and writing – original draft; Jiahao Wan: data curation and visualization, Lehui Liu: data curation; Chunxiang Wu: data curation; Ping Wang: data curation; Xingxing Jiang: formal analysis, writing – review & editing and supervision; Zheshuai Lin: software; Hongming Liu: funding acquisition, writing – review & editing and supervision.

Conflicts of interest

There are no conflicts to declare.

Acknowledgements

The authors are thankful for financial support from the National Natural Science Foundation of China (grant no. 22105046) and the Natural Science Foundation of Guangxi Province (no. 2022GXNSFBA035484).

References

1 W. Q. Liao, D. Zhao, Y. Y. Tang, Y. Zhang, P. F. Li, P. P. Shi, X. G. Chen, Y. M. You and R. G. Xiong, *Science*, 2019, **363**, 1206–1210.
2 H. Y. Ye, Y. Y. Tang, P. F. Li, W. Q. Liao, J. X. Gao, X. N. Hua, H. Cai, P. P. Shi, Y. M. You and R. G. Xiong, *Science*, 2018, **361**, 151–155.
3 D. F. Eaton, *Science*, 1991, **253**, 281–287.
4 X. Dong, H. Huang, L. Huang, Y. Zhou, B. Zhang, H. Zeng, Z. Lin and G. Zou, *Angew. Chem., Int. Ed.*, 2024, **63**, e202318976.
5 X. Wang, X. Leng, Y. Kuk, J. Lee, Q. Jing and K. M. Ok, *Angew. Chem., Int. Ed.*, 2024, **63**, e202315434.
6 L. Qi, X. Jiang, K. Duanmu, C. Wu, Z. Lin, Z. Huang, M. G. Humphrey and C. Zhang, *Angew. Chem., Int. Ed.*, 2023, **62**, e202309365.
7 L. Kang and Z. Lin, *Light:Sci. Appl.*, 2022, **11**, 201.
8 M. Mutailipu, F. Li, C. Jin, Z. Yang, K. R. Poeppelmeier and S. Pan, *Angew. Chem., Int. Ed.*, 2022, **61**, e202202096.
9 H. Tian, N. Ye and M. Luo, *Angew. Chem., Int. Ed.*, 2022, **61**, e202200395.
10 M. Bugajski and M. Malinowski, *Open Phys.*, 2010, **8**, 157–158.

11 D. Cyranoski, *Nature*, 2009, **457**, 953–955.
12 S. Zhao, Y. Yang, Y. Shen, B. Zhao, L. Li, C. Ji, Z. Wu, D. Yuan, Z. Lin, M. Hong and J. Luo, *Angew. Chem., Int. Ed.*, 2017, **56**, 540–544.
13 M. Xia, X. Jiang, Z. Lin and R. Li, *J. Am. Chem. Soc.*, 2016, **138**, 14190–14193.
14 C. Wu, X. Jiang, Z. Wang, L. Lin, Z. Lin, Z. Huang, X. Long, M. G. Humphrey and C. Zhang, *Angew. Chem., Int. Ed.*, 2021, **60**, 3464–3468.
15 C. Wu, C. Jiang, G. Wei, X. Jiang, Z. Wang, Z. Lin, Z. Huang, M. G. Humphrey and C. Zhang, *J. Am. Chem. Soc.*, 2023, **145**, 3040–3046.
16 C. Wu, X. Jiang, Y. Hu, C. Jiang, T. Wu, Z. Lin, Z. Huang, M. G. Humphrey and C. Zhang, *Angew. Chem., Int. Ed.*, 2022, **61**, e202115855.
17 G. Peng, C. Lin, H. Fan, K. Chen, B. Li, G. Zhang and N. Ye, *Angew. Chem., Int. Ed.*, 2021, **60**, 17415–17418.
18 H. Liu, Q. Wu, L. Liu, Z. Lin, P. S. Halasyamani, X. Chen and J. Qin, *Chem. Commun.*, 2021, **57**, 3712–3715.
19 F. You, F. Liang, Q. Huang, Z. Hu, Y. Wu and Z. Lin, *J. Am. Chem. Soc.*, 2019, **141**, 748–752.
20 H. Liu, Q. Wu, X. Jiang, Z. Lin, X. Meng, X. Chen and J. Qin, *Angew. Chem., Int. Ed.*, 2017, **56**, 9492–9496.
21 M. Liang, C. Hu, F. Kong and J. Mao, *J. Am. Chem. Soc.*, 2016, **138**, 9433–9436.
22 N. Ma, J. Chen, B. Li, C. Hu and J. Mao, *Small*, 2023, **19**, 2304388.
23 Q. Chen, C. Hu, J. Chen, Y. Li, B. Li and J. Mao, *Angew. Chem., Int. Ed.*, 2021, **60**, 17426–17429.
24 D. Phanon and I. Gautier-Luneau, *Angew. Chem., Int. Ed.*, 2007, **46**, 8488–8491.
25 E. L. Belokoneva, S. Y. Stefanovich, O. V. Dimitrova, A. S. Karamysheva and A. S. Volkov, *Inorg. Chem.*, 2017, **56**, 1186–1192.
26 D. Phanon, Y. Suffren, M. B. Taouti, D. Benbertal, A. Brenier and I. Gautier-Luneau, *J. Mater. Chem. C*, 2014, **2**, 2715–2723.
27 K. Bouchouit, H. Bougharraf, B. Derkowska-Zielinska, N. Benali-cherif and B. Sahraoui, *Opt. Mater.*, 2015, **48**, 215–221.
28 D. O. Charkin, V. Y. Grishaev, T. A. Omelchenko, E. V. Nazarchuk, S. Y. Stefanovich and O. I. Siidra, *Solid State Sci.*, 2023, **137**, 107116.
29 R. Robert, V. Balisetty, K. Mohanrao, M. Mannamala Pappan, S. Mangalassery, D. Rao and K. Vidyasagar, *Inorg. Chem.*, 2023, **62**, 7890–7897.
30 S. Pal, R. Nagarajan and S. Uma, *Chem. Mater.*, 2023, **35**, 1249–1258.
31 S. Katrych, A. Arakcheeva, A. Sienkiewicz, L. Forró and T. Ivšić, *Inorg. Chem.*, 2021, **60**, 286–291.
32 C. Chen, Y. Wu and R. Li, *Int. Rev. Phys. Chem.*, 1989, **8**, 65–91.
33 N. Ye, Q. Chen, B. Wu and C. Chen, *J. Appl. Phys.*, 1998, **84**, 555.
34 K. M. Ok, P. S. Halasyamani, D. Casanova, M. Llunell, P. Alemany and S. Alvarez, *Chem. Mater.*, 2006, **18**, 3176–3183.
35 P. S. Halasyamani, *Chem. Mater.*, 2004, **16**, 3586–3592.
36 P. S. Halasyamani and K. R. Poeppelmeier, *Chem. Mater.*, 1998, **10**, 2753–2769.
37 M. Kunz and I. D. Brown, *J. Solid State Chem.*, 1995, **115**, 395–406.
38 T. Wu, X. Jiang, K. Duanmu, C. Wu, Z. Lin, Z. Huang, M. G. Humphrey and C. Zhang, *Angew. Chem., Int. Ed.*, 2024, **63**, e202318107.
39 Y. X. Ma, P. F. Li, C. L. Hu, J. G. Mao and F. Kong, *Adv. Sci.*, 2023, **10**, 2304463.
40 Q. Wang, X. H. Dong, L. Huang, K. M. Ok, Z. E. Lin and G. H. Zou, *Small*, 2023, **19**, 2302797.
41 K. Chen, C. Lin, J. Chen, G. Yang, H. Tian, M. Luo, T. Yan, Z. Hu, J. Wang, Y. Wu, N. Ye and G. Peng, *Angew. Chem., Int. Ed.*, 2023, **62**, e202217039.
42 H. X. Tang, Y. X. Zhang, C. Zhuo, R. B. Fu, H. Lin, Z. J. Ma and X. T. Wu, *Angew. Chem., Int. Ed.*, 2019, **58**, 3824–3828.
43 H. Yu, M. L. Nisbet and K. R. Poeppelmeier, *J. Am. Chem. Soc.*, 2018, **140**, 8868–8876.
44 H. Ra, K. M. Ok and P. S. Halasyamani, *J. Am. Chem. Soc.*, 2003, **125**, 7764–7765.
45 M. E. Welk, A. J. Norquist, F. P. Arnold, C. L. Stern and K. R. Poeppelmeier, *Inorg. Chem.*, 2002, **41**, 5119–5125.
46 J. B. Goodenough, *Annu. Rev. Mater. Sci.*, 1998, **28**, 1–27.
47 L. Bindi and C. Cipriani, *Can. Mineral.*, 2003, **41**, 1469–1473.
48 F. C. Zumsteg, J. D. Bierlein and T. E. Gier, *J. Appl. Phys.*, 1976, **47**, 4980–4985.
49 N. E. Brese and M. O'Keeffe, *Acta Crystallogr., Sect. B:Struct. Sci.*, 1991, **47**, 192–197.
50 S. K. Kurtz and T. T. Perry, *J. Appl. Phys.*, 1968, **8**, 3798–3813.
51 C. Wu, T. Wu, X. Jiang, Z. Wang, H. Sha, L. Lin, Z. Lin, Z. Huang, X. Long, M. G. Humphrey and C. Zhang, *J. Am. Chem. Soc.*, 2021, **143**, 4138–4142.
52 Y. Song, X. Hao, C. Lin, D. Lin, M. Luo and N. Ye, *Inorg. Chem.*, 2021, **60**, 11412–11418.
53 K. Chen, Y. Yang, G. Peng, S. Yang, T. Yan, H. Fan, Z. Lin and N. Ye, *J. Mater. Chem. C*, 2019, **7**, 9900–9907.
54 Y. Han, X. Zhao, F. Xu, B. Li, N. Ye and M. Luo, *J. Alloys Compd.*, 2022, **902**, 163727.
55 X. Dong, L. Huang, H. Zeng, Z. Lin, K. M. Ok and G. Zou, *Angew. Chem., Int. Ed.*, 2022, **61**, e202116790.
56 R. E. Perez-D'Gregorio and R. K. Miller, *Teratology*, 1988, **37**, 307–316.
57 N. Kanematsu, M. Hara and T. Kada, *Mutat. Res.*, 1980, **77**, 109–116.
58 B. E. Sørensen, *Eur. J. Mineral.*, 2013, **25**, 5–10.
59 Y. Shang, J. Xu, H. Sha, Z. Wang, C. He, R. Su, X. Yang and X. Long, *Coord. Chem. Rev.*, 2023, **494**, 215345.
60 W. Huang, S. Zhao and J. Luo, *Chem. Mater.*, 2022, **34**, 5–28.
61 P. Li, C. Hu, Y. Li, J. Mao and F. Kong, *J. Am. Chem. Soc.*, 2024, **146**, 7868–7874.
62 T. Wu, X. Jiang, K. DuanMu, C. Wu, Z. Lin, Z. Huang, M. G. Humphrey and C. Zhang, *Adv. Sci.*, 2024, **11**, 2306670.
63 W. M. Sinton, *J. Opt. Soc. Am.*, 1961, **51**, 1301–1309.
64 P. Li, C. Hu, F. Kong, S. Ying and J. Mao, *Inorg. Chem. Front.*, 2021, **8**, 164–172.
65 L. Kang, D. M. Ramo, Z. S. Lin, P. D. Bristowe, J. G. Qin and C. T. Chen, *J. Mater. Chem. C*, 2013, **1**, 7363–7370.